Drought impact in the Bolivian Altiplano agriculture associated with El Niño Southern Oscillation using satellite imagery data

Claudia Canedo-Rosso[1,2], Stefan Hochrainer-Stigler[3], Georg Pflug[3,4], Bruno Condori[5], and Ronny Berndtsson[1,6]

[1]Division of Water Resources Engineering, Lund University, P.O. Box 118, SE-22100 Lund, Sweden
[2] Instituto de Hidráulica e Hidrología, Universidad Mayor de San Andrés, Cotacota 30, La Paz, Bolivia
[3] International Institute for Applied Systems Analysis (IIASA), Schlossplatz 1, A-2361 Laxenburg, Austria
[4] Institute of Statistics and Operations Research, Faculty of Economics, University of Vienna, Oskar-Morgenstern-Platz 1, 1090 Wien, Austria
[5]Inter-American Institute for Cooperation on Agriculture (IICA), Defensores del Chaco 1997, La Paz, Bolivia.
[6] Center for Middle Eastern Studies, Lund University, P.O. Box 201, SE-22100 Lund, Sweden.

Correspondence to: Claudia Canedo-Rosso (canedo.clau@gmail.com)

Abstract. Drought is a major natural hazard in the Bolivian Altiplano that causes large agricultural losses, especially during a positive El Niño-Southern Oscillation (ENSO) phase. Empirical data for drought assessment purposes in this area are scarce and spatially uneven distributed. Due to these limitations we tested the performance of satellite imagery products for providing vegetation, land surface temperature (LST), precipitation and air temperature data on a local level. With this information, the Normalized Difference Vegetation Index (NDVI) and LST were used to classify drought events, associated with past ENSO phases. It was found that the most severe drought events generally occur during positive ENSO phase (El Niño years). We found that a decrease in vegetation is mainly driven by low precipitation and high temperature, and we identified areas where agricultural losses will be most pronounced under such conditions. The results show that droughts can be monitored using satellite imagery data when ground data are scarce or of poor data quality. The results can be especially beneficial for emergency response operations and for enabling a pro-active approach to disaster risk management against droughts.

Keywords: Drought, agriculture, ENSO, NDVI, land surface temperature, climate variables, precipitation, and air temperature.

1. Introduction

Agricultural production is highly sensitive to weather extremes, including droughts and heat waves. Losses due to such hazard events pose a significant challenge to farmers as well as governments worldwide (UNISDR, 2009, 2015). Worryingly, the scientific community predicts an amplification of these negative impacts due to future climate change (IPCC, 2013). Especially in developing countries such as Bolivia, drought is a major natural hazard and Bolivia has experienced large socio-economic losses in the past due to such events (UNDP, 2011; Garcia and Alavi, 2018). However, the impacts vary on a seasonal and annual timescale, in regards to the hazard intensity, as well as the existing capacity to prevent and respond to droughts (UNISDR, 2009, 2015). Regarding the former, the El Niño Southern Oscillation (ENSO) plays an especially important role in several regions of the world, including the Bolivian Altiplano, as it drives losses of agricultural crops, and causes increased food insecurity (Kogan and Guo, 2017). Most important rainfed crops in the region include quinoa and potato (Garcia et al., 2007). Generally speaking, agricultural productivity in the Bolivian Altiplano is low due to adverse weather and poor soil conditions (Garcia et al., 2003). On the other hand, low agricultural production levels can also be associated with the ENSO climate phenomena (Buxton et al., 2013). For this area, droughts are generally driven by the ENSO warm phases (Thompson et al., 1984; Garreaud and Aceituno, 2001; Vicente-Serrano et al., 2015). Previous research has addressed the influence of ENSO on agriculture in South America and the globe (see Iizumi et al., 2014; Ramirez-Rodrigues et al., 2014; Anderson et al., 2017). These studies were calling for a better understanding of the association between ENSO and agriculture to improve crop management practices and food security.

The implementation of drought risk management approaches is now seen as fundamental (see e.g., the Sustainable Development Goals or the Sendai Framework for Risk Reduction) for sustainable development in vulnerable regions, including Latin American countries such as Bolivia (Verbist et al., 2016). To lessen the long-term impacts of these extreme events, the national government in Bolivia has taken several steps, e.g., to allocate budgets for emergency operations to compensate part of the losses occurred. Most of these measures are implemented ex-post (i.e., after a disaster event). However, based on ENSO forecasting, an El Niño event can be predicted 1 to 7 months ahead (Tippett et al., 2012) and consequently, there is an opportunity to implement additional ex-ante policies (i.e., before the event) to reduce societal impacts to droughts, increase preparedness, and generally improve current risk management strategies.

One major constraint for drought risk management in Bolivia is the scarce and uneven distribution of weather and agricultural production related ground data. To circumvent this problem, we test satellite-based data products

(compared to available empirically gauged data) to provide a full coverage (in respect to land area) for drought assessment and its spatial distribution across the region. Due to the particular importance of ENSO for drought risk management, we additionally assess the impacts associated with ENSO on agriculture for the Bolivian Altiplano. Furthermore, we give indications what climate variables may be most important in which regions to predict drought losses that can further be used for hotspot selection. The paper is organized as follows, section 2 presents the methodology applied and data used, and section 3 presents the corresponding results found. Section 4 puts the results into a context of drought impact and hotspot selection with conclusion.

2. Data Used and Methodology

2.1 Ground data and satellite imagery

The methodology applied is very much related to the data scarce situation for the Bolivian Altiplano and we therefore start with an introduction of available datasets that are used for our purposes. In regard to climate, the Altiplano has a pronounced southwest-northeast precipitation gradient (200–900 mm year^{-1}) during the wet season occurring from November to March (Garreaud et al., 2003). Over 70% of total precipitation occur during summer months (from December to February, see Fig. 1a) in association with the South American Monsoon (see Zhou and Lau, 1998; Garreaud et al., 2003). Time series of monthly precipitation at 12 locations as well as mean, maximum, and minimum temperature at 8 locations from September 1981 to August 2015 were available from the National Service of Meteorology and Hydrology (SENAMHI) of Bolivia (see Table A1). These data sets have less than 10% of missing data.

As already indicated, precipitation and temperature gauge locations are unevenly distributed and mainly concentrated in the northern Bolivian Altiplano. To improve the spatial coverage of climate related data, monthly quasi-rainfall time series from satellite data the Climate Hazards Group InfraRed Precipitation with station data (CHIRPS) were included in our study. CHIRPS represents a 0.05° spatial resolution satellite imagery and a quasi-global rainfall dataset from 1981 to the near present (Funk et al., 2015). The advantage of using CHIRPS is the high spatial resolution of data, obtained with resampling of TMPA 3B42 (with 0.25° grid cell). The spatial resolution represents a better option for agricultural studies as well and therefore is most appropriate for our approach (CHIRPS is described in detailed at http://chg.geog.ucsb.edu/data/chirps/).

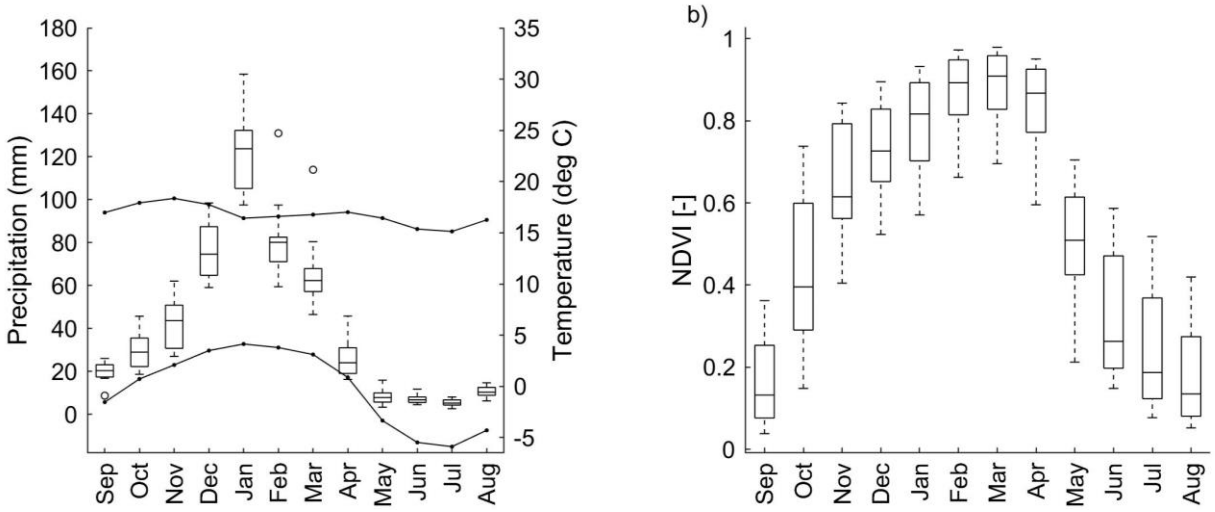

Fig. 1. (a) Gauged mean monthly total precipitation and average maximum and minimum temperature from September 1981 to August 2015. (b) Mean monthly NDVI at the same spatial locations. Lower and upper box boundaries 25th (Q1) and 75th (Q3) percentiles, respectively, line inside box is median, lower and upper error lines 1.5 times the interquartile range (Q3-Q1) from the top or bottom of the box, white circles data falling outside 1.5 times the interquartile rage.

Additionally, satellite monthly mean air temperature was obtained from the Physical Sciences Division (PSD) of the US National Oceanic and Atmospheric Administration (NOAA, https://www.esrl.noaa.gov/psd/) defined by Willmott and Matsuura. The satellite air temperature dataset has a resolution of 0.5° and was available during the study period from September 1981 to August 2015.

Apart from climate datasets, NDVI was assembled from the Advanced Very High Resolution Radiometer (AVHRR) sensors by the Global Inventory Monitoring and Modelling System (GIMMS) at semi-monthly (15 days) time step with a spatial resolution of 0.08°. NDVI 3g.v1 (third generation GIMMS NDVI from AVHRR sensors) was available from September 1981 to August 2015. The NDVI is an index that presents a range of values from 0 to 1, bare soil values are closer to 0, while dense vegetation is close to 1 (Holben, 1986). NDVI 3g.v1 GIMMS provides information to differentiate valid values from possible errors due to snow, cloud, and interpolation. These errors were removed from the dataset and replaced with the nearest neighbour value.

Additionally, Land Surface Temperature (LST) was obtained from the Global Land Data Assimilation System (GLDAS) by the Noah Land Surface Model L4 monthly version 2.0. The LST dataset has a resolution of 0.25°

and it was available for the study period from September 1981 to August 2015. Agricultural land in the Bolivian Altiplano covers about 20,000 km^2, and it was spatially identified based on the land use map developed by the Autonomous Authority of the Lake Titicaca (for the northern Altiplano) in 1995 at a scale of 1:250,000 (UNEP, 1996), and the Ministry of Development Planning in 2002 using Landsat imagery and ground information at a scale 1:1,000,000 (geo.gob.bo, for the southern Altiplano).

2.2 Validation of satellite-based data products

The performance of the satellite-based data (compared to empirical ground data, see Fig. 2) to accurately estimate amount of rainfall (for example to assess rain detection capability) was based on statistical measures for monthly pair-wise time series, including categorical analyses and follows the methodology applied in previous studies in this region for comparison reasons (Blacutt et al., 2015; Satgé et al., 2016). The mean error (ME), bias, and mean absolute error (MAE) were calculated based on Wilks (2006). These measures evaluate the prediction accuracy of the satellite data compared to gauged data. The ME and bias show the degree of over- or underestimation (Duan et al., 2015). In contrast, as measuring the absolute deviation, MAE shows only non-negative values. The ME, bias, and MAE perfect match correspond to zero between gauge observation and satellite-based estimate. Furthermore, and similar to Blacutt et al. (2015) and Satgé et al. (2016), the Spearman's rank correlation was computed to estimate the goodness of fit to observations. To evaluate results, as in similar studies, correlation coefficients larger or equal to 0.7 were considered as reliable (Condom et al., 2011; Satgé et al., 2016). The ME, bias, and MAE were calculated, respectively according to Eqn. (1), (2), and (3) (Table 1).

Table 1. Accuracy measures for satellite data performance evaluation. Here, N is the number of samples, S_i is the satellite-based dataset for month i, and G_i is the gauged dataset for the same month. H is a hit, F is a false alarm, and M is a miss.

Statistical indicator	Abbreviation	Units	Equation	
Mean error	ME	mm, ^{o}C	$\sum(S_i - G_i) \,/\, N$	(1)
Bias	Bias	%	$\sum(S_i - G_i) \,/\, \sum G_i \times 100$	(2)
Mean absolute error	MAE	%	$\sum\lvert(S_i - G_i) \,/\, G_i\rvert \,/\, N \times 100$	(3)
Probability of detection	POD	-	$H \,/\, (H + M)$	(4)
False alarm ratio	FAR	-	$F \,/\, (H + F)$	(5)

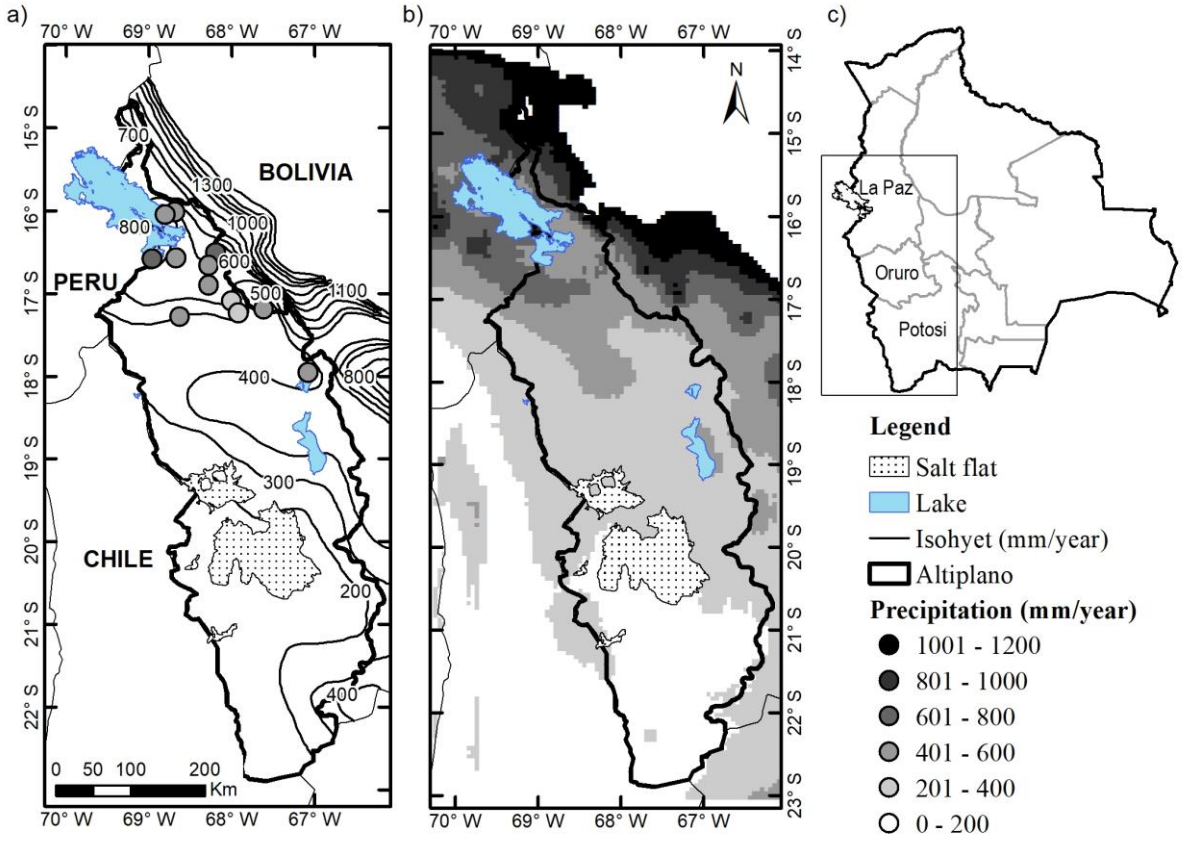

Fig. 2. Mean of total annual precipitation from September 1981 to August 2015 for: (a) gauged precipitation data (circles) and isohyets (solid line), (b) the CHIRPS satellite rainfall product, and (c) Bolivia, and the major political divisions of the Bolivian Altiplano: La Paz, Oruro and Potosi.

Two statistical indicators based on a contingency table were computed for the categorical statistics, namely Probability of Detection (POD) and False Alarm Ratio (FAR). The POD indicates what fraction of the observed events that was correctly estimated, and FAR indicates the fraction of the predicted events that did not occur (Bartholmes et al., 2009; Ochoa et al., 2014; Satgé et al., 2016). The POD and FAR range from 0 to1, where 1 is a perfect score for POD, and 0 is a perfect score for FAR. These measures were used to evaluate the satellite estimations. Here, the rainfall amounts are considered as binary values, i.e., rain occurrence or absence. Based on this approach, three counting variables were taken into account: the number of events when the satellite rain estimation and the rain gauge report a rain event (hit or H), when only the satellite reports a rain event but no rain

on the ground is observed (false alarm or F), and when only the rain gauge reports a rain event but not the satellite and therefore is a miss (M). The POD and FAR were calculated, respectively according to Eqn. (4) and (5) (Table 1).

Besides the precipitation data, satellite temperature data were validated using ground data. The satellite air temperature was correlated with the mean gauged temperature at the same spatial location. The mean temperature of the gauged data was calculated using the arithmetic mean between the maximum and minimum temperature. The regression performance was evaluated using the monthly pair wise time series to define the Spearman's rank correlation, relative ME, bias, and MAE.

2.3 Drought associated with ENSO

Healthy vegetation usually shows enlarged near infrared and reduced visible red band, and shows a low surface temperature due to the absorption of thermal infrared radiation (Kogan and Guo, 2017). Therefore, vegetation indices and land surface temperature (LST) are widely used for water and energy balance approaches (see Moran et al., 1994; Corbari et al., 2010; Sánchez et al., 2012; Helman et al., 2015). Previous findings indicate a negative (positive) relationship between LST and NDVI caused by limited moisture (energy-temperature) availability for vegetation growth (Karnieli et al., 2010). Drought spells typically present low NDVI and high LST due to vegetation deterioration and higher contribution of the soil signal (Kogan, 2000). Here, we study the relationship between LST and NDVI using the Vegetation Health Index (VHI, Eqn. (8)) developed by Kogan (1995) that combines the Vegetation Condition Index (VCI, Eqn. (6)) and Temperature Condition Index (TCI, Eqn. (7)). VCI is a normalized NDVI that allows to seek the variability of the signal, showing an increased VCI when NDVI increases. (Kogan, 1995; Kogan, 2000; Kogan and Guo, 2017). In contrast, the TCI formulates a reverse ratio compared to the VCI, decreasing when LST increases, assuming that higher land surface temperatures suggest a decreasing soil moisture causing stress of the vegetation canopy.

Table 2. Drought classification indices.

Drought index	**Acronym**	**Equation**	
Vegetation Condition Index	VCI	$(NDVI_i - NDVI_{min}) \,/\, (NDVI_{max} - NDVI_{min})$	(6)
Temperature Condition Index	TCI	$(LST_{max} - LST_i) \,/\, (LST_{max} - LST_{min})$	(7)
Vegetation Health Index	VHI	$0.5\ VCI + 0.5\ TCI$	(8)

where NDVIi, NDVImax and NDVImin (LST, LSTmax and LSTtmin) are monthly NDVI (LST) and the month absolute maximum and minimum from September 1981 to August 2015, respectively. We took a mean of VCI and TCI assuming that they equally contribute to the VHI.

The VCI, TCI, and VHI was defined for each month during the growing season (from September to April). We assumed the occurrence of drought event when the indices were lower than 40%. The classification of drought was established based on the severity of the event in which five classes were defined: extreme (≤10), severe, (≤20), moderate (≤30), mild (≤40), and no (>40) drought (Bhuiyan and Kogan, 2010).

The drought events were further classified based on the occurrence of El Niño and La Niña events (Table 3). The classification ENSO was obtained from Null (2018). El Niño and La Niña events were identified from 5 consecutive overlapping 3-month mean sea surface temperature for the Niño 3.4 region (in the tropical Pacific Ocean). A moderate El Niño (La Niña) was defined as 5 consecutive overlapping 3-month periods at or above the +1.0 º to + 1.4 ºC anomaly (-1.0 º to -1.4 ºC), strong El Niño (La Niña) event for a threshold between +1.5 º to +1.9 ºC anomaly (-1.5 º to -1.9 ºC anomaly), and a very strong El Niño event for a threshold equal or greater than +2 ºC anomaly (https://ggweather.com/enso/oni.htm). For this study, a neutral or weak phase was defined as a threshold between -0.9 º to +0.9 ºC anomaly.

Table 3. El Niño and La Niña phases (from Null (2018)).

El Niño			La Niña	
Moderate	**Strong**	**Very Strong**	**Moderate**	**Strong**
1986-87	1987-88	1982-83	1995-96	1988-89
1994-95	1991-92	1997-98	2011-12	1998-99
2002-03		2015-16		1999-00
2009-10				2007-08
				2010-11

2.4 Regression of vegetation and climate variables

A stepwise regression approach was used to quantify the dependency between vegetation and satellite-based climate variables (precipitation and temperature; Eqn. 10) further to be used for hotspot selection. In more detail, the results presented here are a combination of forward and backward selection techniques to increase the robustness of the results (in terms of explanatory power, i.e., variability explained, as well as variable selection, i.e., same variable selected across a range of possible models). The independent variable considered was NDVI,

and the dependent variables were selected to include precipitation and air temperature (for the same spatial location across the study region). We assumed that NDVI represents the crop phenological stages of the growing season that is from September to April (Fig. 1). Precipitation was selected as predictor due to its relevance for water availability for vegetation growth. Precipitation is the main source of water in the Altiplano because only 9% of the Bolivian cropped surface area are irrigated (INE, 2015). Air temperature is a relevant variable due to photosynthetic and respiration processes (Karnieli et al., 2010). Firstly, the NDVI was related to CHIRPS rainfall datasets. Secondly, air temperature was included in the analysis. For this, only the NDVI grids for agricultural land were selected. Since, agricultural production data are scarce in the region, we suggest that crop yield data can be improved using the NDVI. Besides improving the crop yield resolution, the NDVI also allows to analyse the variability of vegetation at a monthly time scale. This makes it possible to analyse the phenology of the studied crops through to the growth phases. NDVI estimates the vegetation vigour (Ji and Peters, 2003) and crop phenology (Beck et al., 2006). The final regression model therefore is

$$NDVI = \beta_0 + \beta_1\, precipitation + \beta_2 air\ temperature \quad (10)$$

For the forward selection, the variables were entered into the model one at a time in an order determined by the strength of their correlation with the criterion variable (only including variables if they present a confidence level of 95%). The effect of adding each variable was assessed during its entering stage, and variables that did not significantly add to the fit of the model were excluded (Kutner et al., 2004). For backward selection, all predictor variables were entered into the model first. The weakest predictor variable was then removed and the regression fit re-calculated. If this significantly weakened the model then the predictor variable was re-entered, otherwise it was deleted. This procedure was repeated until only useful predictor variables (in a statistical sense, e.g., significant as well as model fit) remained in the model (Rencher, 1995). The results were compared with results from literature regarding phenology and weather-related characteristics of crops.

It should be noted that the precipitation in the Altiplano shows a marked rainy season from November to March. The peak of precipitation is in December and January (Fig. 1a). And, NDVI displays a peak in March and April (Fig. 1b). The lag between the precipitation and NDVI is reasonable since vegetation requires time to grow (e.g., Shinoda, 1995; Cui and Shi, 2010; Chuai et al., 2013). Considering this lag-time, the 3-month time series of NDVI was regressed with the 3-month time series of the climate variables (satellite-based data products of precipitation and air temperature) during the growing period for the agricultural land. First, the NDVI and the climate variables were related considering the overlapped 3-month time series, and afterwards a relation was developed considering a lag from 1 to 4 months between NDVI and climate variables, resulting 22 regressions per NDVI grid. The

regressions were developed for each NDVI grid separately, associated with the nearest precipitation and air temperature dataset. Previous to the stepwise regression analysis, the 3-month time series of NDVI, satellite precipitation and satellite air temperature data were standardized.

3. Results

Validation of the satellite rain data using empirical precipitation data from the weather stations was done for the 12 locations where gauge precipitation data were available (see Fig. 2 and Table A1). The qualitative methods discussed in section 2.2 for the CHIRPS rainfall estimates show differences between summer (from December to March) and winter season (from June to August). CHIRPS data show better accuracy during summer. The precipitation during the austral summer is highly relevant because it concentrates the 70% of the annual rainfall (Garreaud et al., 2003) and it occurs during the growing season. During May, CHIRPS data show lower accuracy compared to the other months. The precipitation from May to August is almost null in the study area (Fig. 1) and it will be further described as the dry season. This season presents stable atmospheric conditions with few precipitation events (Garreaud et al., 2003).

Interestingly, the spearman rank correlation between monthly gauged precipitation and satellite rain product datasets was significant (p-value <0.05) for all locations. The correlation coefficients (r) vary from 0.5 to 0.8 (mean = 0.7). The ME and bias disclose an underestimation of precipitation estimation during October, November, and April, and an overestimation during the summer season (mean = 5 mm and 7%, respectively) with a peak in February. For the MAE coefficient, CHIRPS estimations are more accurate during the rainy season (mean = 31%). In contrast, CHIRPS data indicate poor accuracy during the dry season (mean MAE = 92%). From June to August, CHIRPS data present an underestimation of the gauged precipitation (mean bias = -39%). Summarizing these observations, we conclude that the CHIRPS-rainfall dataset is more accurate during the rainy season, and it represents an adequate alternative in case of lack of gauged data or in case of poor data quality. However, it should be noted that such data still must be used with caution considering the uncertainties due to the under or overestimation of precipitation along the heterogeneous topography of the Altiplano (see Paredes-Trejo et al., 2016; Paredes-Trejo et al., 2017; Rivera et al., 2018).

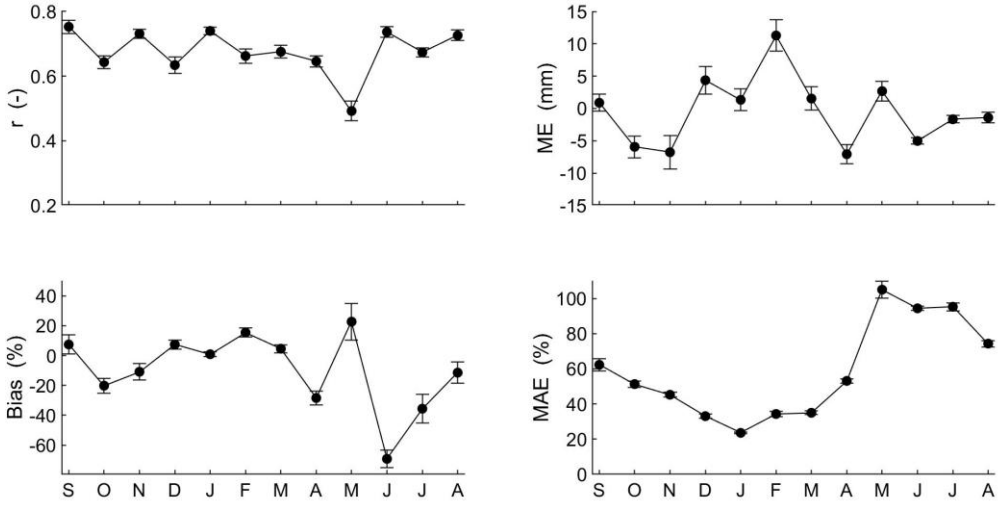

Fig. 3. Monthly accuracy measures of CHIRPS-rainfall data product. Mean monthly values are represented by black circles, and bars represent the standard error of the mean.

Moving from rainfall to temperature, the inter-annual temperature at the 8 locations varied considerably between summer (from December to March) and winter (from June to August), including a larger variance for the minimum temperature (Fig. 1a). The mean monthly air temperature from satellite data was compared with mean temperature of gauged data. The satellite air temperature underestimated the mean gauged temperature, and this error could be due to the high elevation and cloud coverage. The spearman correlation at the 8 stations displayed coefficients from 0.1 to 0.7. From November to April, air temperature satellite-based estimations show significant correlations (p-value <0.05). Large correlations are shown during summer season (mean = 0.7), while the other months show rather weak correlations. ME and bias show a slight underestimation from October to April (mean = -0.5 and -4% respectively), and an overestimation from May to August (mean = 0.3 and 12% respectively). Finally, MAE is about 10% from September to April, higher values develop during winter season (mean = 32%). In conclusion, the satellite air temperature data product performs better from November to April. Similar to the precipitation data, the application of satellite air temperature data must take into account the potential errors due to the estimation uncertainties, mainly during winter season.

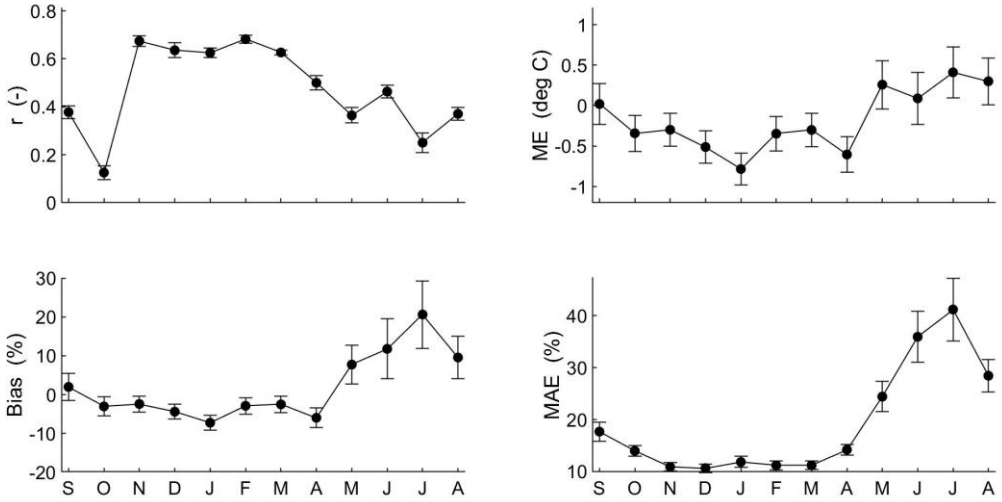

Fig. 4. Same as Fig. 3 but for accuracy measures of satellite-based air temperature data product.

As discussed above, the VCI, TCI, and VHI were calculated during the growing season. The sowing period depends on the initial soil moisture content, therefore the beginning of the growing season oscillates from September to November (Garcia et al., 2015). For this reason, the drought severity was classified considering the mean of VCI, TCI, and VHI for the agricultural land during November-April. Figure A1 shows mean monthly VCI from November 1981 to April 2015. The major drought events (severe or extreme) are visible in 1982-83, 1983-84, and 2009-10. Followed by moderate drought events during 1987-88, and 1993-94, and several mild events. Figure A2 shows the mean monthly TCI, where the major drought events (severe or extreme) occurred in 1982-83, 1987-88, 1997-98, 2004-05, and 2009-10. Followed by moderate drought events during 1981-82, 1983-84, 1994-95, 2006-07, and 2008-09, and several mild events as well. Finally, Fig. A3 shows the VHI results, in which the major drought events occurred during 1982-83, 2004-05, and 2009-10.

Further, we related drought indices with the ENSO phases (Table 4). Extreme, and severe droughts were generally found during El Niño phase. The extreme drought of 1982-83, coincided with a very strong El Niño phase. For this event, the largest economic losses caused by droughts during the study period were reported (Table 5). Followed by the very strong El Niño phase of 1997-98, which reported the second largest economic losses. Besides these two main drought events, the strong El Nino 1987-88 coincided with an extreme/moderate drought (TCI≤10%, VCI≤30%) classification. During this period, large economic losses were reported as well (Table 5). In contrast, the strong El Niño 1991-92 showed low severity (mild drought VCI≤40%), and no economic losses

were reported. This indicates that despite El Niño phenomenon is generally associated with drought in the Altiplano, there are several other mechanisms that drive a drought occurrence and determine its severity. For instance, dry (wet) and warm (cool) conditions during El Niño (La Niña) phases are generally shown in the tropics (Garreaud et al., 2003). However, an anomalous location and intensity of zonal wind anomalies could cause disturbances of the warming and cooling air patterns causing rainfall anomalies on the Altiplano (Garreaud and Aceituno, 2001). This is the case of the dry La Niña 1988-89 that showed a mild drought classification (TCI≤40%).

Table 4. Drought indices classification during ENSO phases.

ENSO	Drought	VCI	TCI	VHI
El Niño	Extreme		1982-83, 1987-88, 1997-98	
	Severe	1982-83, 2009-10	2009-10	1982-83, 2009-10
	Moderate	1987-88	1994-95	
	Mild	1986-87, 1991-92	1986-87	1994-95, 1997-98
La Niña	Mild	1995-96, 2007-08, 2010-11	1988-89	
Neutral/ weak	Extreme		2004-05	
	Severe	1983-84		
	Moderate	1993-94	1981-82, 1983-84, 2006-07, 2008-09	2004-05
	Mild	1981-82, 1996-97, 2003-04, 2008-09	1984-85 1990-91 1993-94 2014-15	1981-82, 1983-84, 1990-91, 1993-94, 2005-06, 2008-09

One severe (1983-84) and one extreme (2004-05) event occurred during a neutral/weak ENSO. The severe drought (VCI ≤ 20%) occurred during a neutral phase of 1983-84. This coincides with the findings of Vicente-Serrano et al. (2015), that analyzed the standardized precipitation/evaporation index in Bolivia, which is an alternative technique to characterize a meteorological drought. The extreme drought (TCI ≤ 10%) of 2004-05 occurred in November and December. From January to April of 2004-05 the VCI and VHI were above 40%, and there were no claims of drought losses in the Altiplano for this particular year (Table 5). Besides these two events, moderate and mild droughts also occurred during non El Niño phases.

Table 5 shows that five drought events were reported during a neutral ENSO phase. In 2012-13, the largest impact occurred, affecting about 80 000 people in the Altiplano (Desinventar, 2020). Despite that the mean of the drought indices indicates no drought during this period (VCI, TCI, and VHI >40%), some spatial locations in the study

region indicated the occurrence of a drought event in November and December (21% and 29% of the total studied grids showed mild and moderate droughts for the TCI and VCI respectively).

Table 5. Drought impact in Bolivia (from EM-DAT (2020), BID (2016), and CAF (2000)).

Year	ENSO phase	Affected people	Total damage ('000 US$)
1982-83	El Niño	3 083 049	917 200
1987-88	El Niño		48 400
1989-90	Neutral	283 160	
1997-98	El Niño		279 310
1993-94	Neutral	50 000	
1999-00	La Niña	20 000	
2003-04	Neutral	55 000	
2007-08	La Niña	27 500	
2009-10	El Niño	62 500	100 000
2012-13	Neutral	340 355	
2013-14	Neutral	51 180	

Regarding the relationship between vegetation and climate variables, we note that the precipitation season occurs mainly during the austral summer months (from December to March), and the vegetation development shows a lag with a maximum development of about March and April (Fig. 1). The NDVI (Fig. 1b) shows a similar growing pattern as the crop phenology in the region, which starts in September and ends in April. Maximum and minimum temperature varies during the year. Higher temperature during the austral summer leads to higher evapotranspiration and a decrease of water retained in the root zone. With this presumption, stepwise linear regression models were tested using 3-month time series of NDVI as dependent variable and 3-month time series of satellite-based data product of precipitation and air temperature as independent variables (Eqn. (10)). The stepwise regression was defined considering the overlapped 3-month time series, and the 3-month time series with a lag from 1 to 4 months at the same spatial location over the agricultural land.

The results of the stepwise regression show larger coefficient of determination (R^2) in the northern and central Bolivian Altiplano, starting from the southern Lake Titicaca and moving southwards to the Lake Poopó, and close to the rivers paths. Lower R^2 is shown along the southwestern Bolivian Altiplano, that could be explained through the large variance of the NDVI, which may depend to on other factors besides precipitation and temperature, including crop management. Figure 5 shows the R^2 of the best fit regression in the Bolivian Altiplano for the

three-month period of NDVI and the climate variables (precipitation and temperature) during the beginning and end of the growing season. It can be seen that the NDVI depends largely on the studied climate variables. This may be due to the crop´s sensitivity for water stress during specific stages of the growing season. For instance the most sensitive stages of the quinoa crop are the emergence, flowering, and grain development (see Geerts et al., 2008; Geerts et al., 2009), and the near absence of irrigation practices in most of these regions.

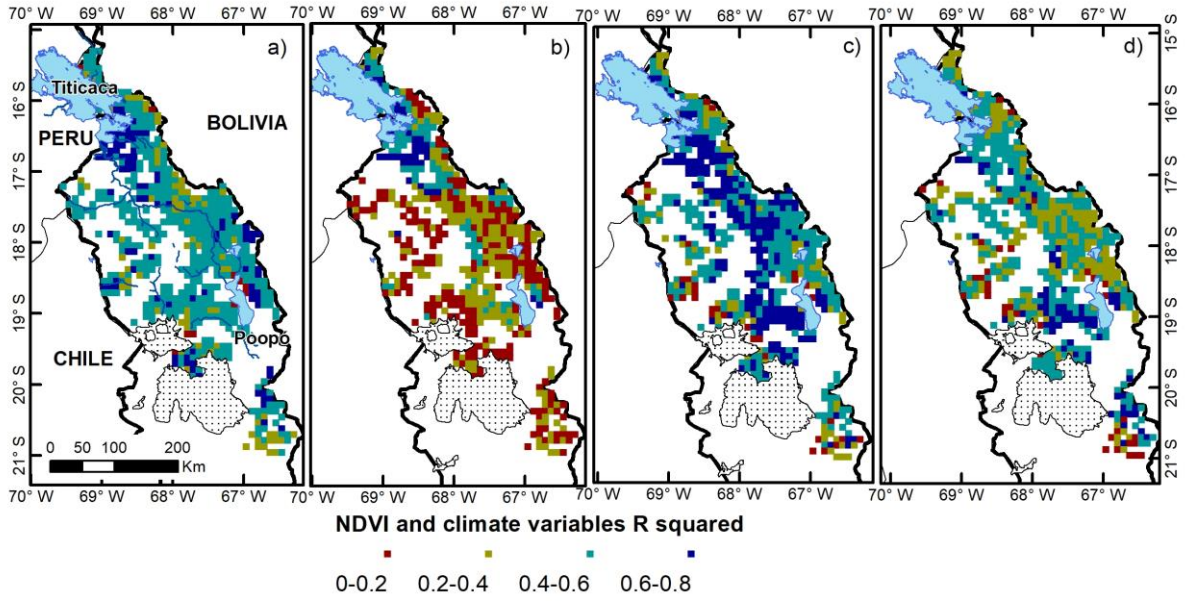

Fig. 5. Coefficient of determination (R^2) of NDVI for the 3-month time series for a) SON, b) OND, c) MAM and d) MAM and the climate variables (satellite precipitation and air temperature products) for SON, SON, FMA, and MAM respectively. The significant regression coefficients for precipitation (air temperature) cover: a) 45% (98%), b) 64% (91%), c) 95% (96%), and d) 23% (98%) of the total studied grids that represent the agricultural land.

In more detail, the stepwise regression results for the overlapping 3-month time series of NDVI and climate variables for SON (September, October, and November) show statistically significant coefficients for precipitation and air temperature at 45% and 98% the agricultural area in the Bolivian Altiplano with a median of 0.2 and 0.7, respectively (Fig. 5a). This indicates that the NDVI increases with more rain and higher air temperature. Interestingly, the significant regression coefficients of NDVI for OND (October, November, and December) associated with precipitation and air temperature for SON cover 64% and 91% of the agricultural area, and have a positive median of 0.3 and 0.4, respectively (Fig. 5b). A time-lag of one month shows larger spatial coverage of

response of vegetation to precipitation anomalies. Here, the largest coefficient of determination are shown in areas surrounding the Lake Titicaca. Moreover, the response of the NDVI for MAM (March, April, and May) to the studied climate anomalies for FMA (February, March and April) covers 95% and 96% of the agricultural land for precipitation and air temperature, respectively (Fig. 5c). This mostly shows coefficients of determination ranging from 0.4 to 0.8, and positive regression coefficients for precipitation and air temperature have a median of 0.5 and 0.4, respectively. The hours of sun required for crop development could be the explanation for the time-lag between vegetation and the climate variables. In addition, the lag differences between vegetation and precipitation can be explained by topography, land cover, ground-water, and soil properties (Yarleque et al., 2016). Finally, the regression for NDVI and climate variables for the overlapped 3-month time series of MAM shows significant coefficients at 23% and 98% of the agricultural land, with a median of 0.4 and 0.6 for precipitation and air temperature, respectively (Fig. 5d). Hence, the vegetation response to precipitation is limited for the last overlapped 3-month time series of the growing season. However, it should be noted that air temperature remains an important variable.

To summarize, while acknowledging some important limitations, we found the CHIRPS dataset adequate to be used for drought risk assessment in case of severe data scarcity for the Bolivian Altiplano. Furthermore, we found that the vegetation variance can be explained by precipitation and air temperature. More specifically, we point out the relevance of precipitation as the main water source for vegetation development and air temperature as a driver of photosynthetic processes. Precipitation is particularly important at the early and late phenological stages, in which crops are more sensitive to water shortage. This is the case for the main crops in region, i.e., quinoa and potato. For the quinoa crop, the most sensitive phases to water stress are the emergence, flowering, and grain development (see Geerts et al., 2008; Geerts et al., 2009). The most sensitive phases of the potato crop to water stress is the tuber initiation and bulking (van Loon, 1981; Alva et al., 2012). On the other hand, air temperature is relevant for vegetation productivity, and overall, we found a positive relation between vegetation and air temperature. However, in prolonged dry periods, high air temperature could increase the evapotranspiration rates, and in consequence, decrease the soil moisture (Huang et al., 2019). This scenario could impact negatively the vegetation, as this is the case of the drought events of 1982-83 and 1997-98, where large production losses were reported (Santos, 2006).

4. Discussion and Conclusion

We employed a satellite dataset product and tested its empirical accuracy as well as performance to similar (but with coarser resolution) datasets available for the Bolivian Altiplano region. Afterwards spatio-temporal patterns of satellite precipitation and air temperature anomalies were explored based on monthly time series during the period of September 1981 to August 2015. Drought severity was evaluated based on a drought classification scheme using NDVI and LST. Finally, association between the spatial distribution of NDVI with precipitation and air temperature was examined. Using these datasets, it was shown that drought risk (measured through various drought indices) increases substantially during El Niño years (Table 4 and 5), and as a consequence the socio-economic vulnerability of farmers will likely increase during such periods. ENSO forecasts as well as drought severity (through drought indices) can help to determine possible hotspots of crop deficits during the growing season. Through empirical relationship with climate variables on the local scale our approach can enable a pro-active approach to disaster risk management against droughts. As it was shown here, ENSO warm phase related characteristics are especially important in the context of extreme drought events and could therefore be incorporated within early warning systems as standard practice. Despite these challenges for development of drought early warning systems (see FAO, 2016, 2017), applications have been successful in the past (e.g., Global Information and Early Warning System (GIEWS) of FAO, and Famine Early Warning System (FEWS) of USAID). Monitoring and predicting ENSO can therefore significantly contribute to reduce the risk of disasters. This study is a first attempt to provide an assessment of drought impact on agriculture in relation to the ENSO phenomenon for the Bolivian Altiplano. We focused on where vegetation is more affected by droughts over agricultural land and how this can be clarified using satellite imagery. It is important to note that the variance of drought indices (as well as NDVI) to a large extend is explained by precipitation and air temperature anomalies in the studied region. The agriculture in this semi-arid region is ecologically fragile and the main water source is precipitation, and thus crop production is considerably affected by precipitation anomalies. However, while an overall response of vegetation variance to precipitation and air temperature is evident, it is important to consider other variables, such as evapotranspiration and soil moisture to improve risk-based models. Another important issue is the time-lag of the response of vegetation to precipitation and air temperature anomalies, which shows a hysteresis of 1-2 months. These findings provide information for future drought risk management and early warning system applications. In addition, with such information agricultural models can be set up and risk management plans with better accuracy determined.

Acknowledgements

The authors want to thank the staff at the International Institute for Applied System Analysis (IIASA), in particular the Young Scientist Summer Program (YSSP) 2017, where this study was conceived. This research was supported by the Swedish International Development Cooperation Agency (SIDA), and the FORMAS Research Council for Environment, Landscaping and Urban Development. The authors would like to express their gratitude the Servicio Nacional de Meteorología e Hidrología (SENAMHI) for providing the meteorological data. The authors would also like to thank Ramiro Pillco Zolá and Ángel Aliaga Rivera for the coordination of the research project with the Universidad Mayor de San Andrés of Bolivia.

References

Alva, A. K., Moore, A. D., and Collins, H. P.: Impact of Deficit Irrigation on Tuber Yield and Quality of Potato Cultivars, Journal of Crop Improvement, 26, 211-227, 10.1080/15427528.2011.626891, 2012.

Anderson, W., Seager, R., Baethgen, W., and Cane, M.: Life cycles of agriculturally relevant ENSO teleconnections in North and South America, Int. J. Climatol., 37, 3297-3318, doi:10.1002/joc.4916, 2017.

Bartholmes, J. C., Thielen, J., Ramos, M. H., and Gentilini, S.: The european flood alert system EFAS – Part 2: Statistical skill assessment of probabilistic and deterministic operational forecasts, Hydrol. Earth Syst. Sci., 13, 141-153, 10.5194/hess-13-141-2009, 2009.

Beck, P. S. A., Atzberger, C., Høgda, K. A., Johansen, B., and Skidmore, A. K.: Improved monitoring of vegetation dynamics at very high latitudes: A new method using MODIS NDVI, Remote Sens. Environ., 100, 321-334, 10.1016/j.rse.2005.10.021, 2006.

Bhuiyan, C., and Kogan, F. N.: Monsoon variation and vegetative drought patterns in the Luni Basin in the rain-shadow zone, Int J Remote Sens, 31, 3223-3242, 10.1080/01431160903159332, 2010.

BID: Analisis ambiental y social, in: Programa de Saneamiento del Lago Titicaca, Banco Interamericano de Desarrollo (BID), La Paz, Bolivia, 2016.

Blacutt, L. A., Herdies, D. L., de Gonçalves, L. G. G., Vila, D. A., and Andrade, M.: Precipitation comparison for the CFSR, MERRA, TRMM3B42 and Combined Scheme datasets in Bolivia, Atmospheric Research, 163, 117-131, 10.1016/j.atmosres.2015.02.002, 2015.

Buxton, N., Escobar, M., Purkey, D., and Lima, N.: Water scarcity, climate change and Bolivia: Planning for climate uncertainties, SEI discussion brief, Stockholm Environment Institute, Davis, USA, 4 pp., 2013.

CAF: Las lecciones de El Niño, Bolivia. Memorias del fenómeno El Niño 1997-1998, retos y propuestas para la región andina., Corporación Andina de Fomento (CAF), Caracas, Venezuela, 2000.

Chuai, X. W., Huang, X. J., Wang, W. J., and Bao, G.: NDVI, temperature and precipitation changes and their relationships with different vegetation types during 1998–2007 in Inner Mongolia, China, Int. J. Climatol., 33, 1696-1706, 10.1002/joc.3543, 2013.

Condom, T., Rau, P., and Espinoza, J. C.: Correction of TRMM 3B43 monthly precipitation data over the mountainous areas of Peru during the period 1998–2007, Hydrol. Process., 25, 1924-1933, 10.1002/hyp.7949, 2011.

Corbari, C., Sobrino, J. A., Mancini, M., and Hidalgo, V.: Land surface temperature representativeness in a heterogeneous area through a distributed energy-water balance model and remote sensing data, Hydrol. Earth

Syst. Sci., 14, 2141-2151, 10.5194/hess-14-2141-2010, 2010.
Cui, L., and Shi, J.: Temporal and spatial response of vegetation NDVI to temperature and precipitation in eastern China, Journal of Geographical Sciences, 20, 163-176, 10.1007/s11442-010-0163-4, 2010.
Duan, Y., Wilson, A. M., and Barros, A. P.: Scoping a field experiment: error diagnostics of TRMM precipitation radar estimates in complex terrain as a basis for IPHEx2014, Hydrol. Earth Syst. Sci., 19, 1501-1520, 10.5194/hess-19-1501-2015, 2015.
FAO: 2015-2016 El Nino early action and response for agriculture, food security and nutrition, 43, 2016.
FAO: Global early warning - Early action report on food security and agriculture July-September 2017, Early Warning – Early Action (EWEA), Agricultural Development Economics Division (ESA), and Food and Agricultural Organization of the United Nations (FAO), Rome978-92-5-109806-6, 27, 2017.
Funk, C., Peterson, P., Landsfeld, M., Pedreros, D., Verdin, J., Shukla, S., Husak, G., Rowland, J., Harrison, L., Hoell, A., and Michaelsen, J.: The climate hazards infrared precipitation with stations—a new environmental record for monitoring extremes, A Nature Research Journal, 2, 150066, 10.1038/sdata.2015.66, 2015.
Garcia, M., Raes, D., and Jacobsen, S.-E.: Evapotranspiration analysis and irrigation requirements of quinoa (Chenopodium quinoa) in the Bolivian highlands, Agric. Water Manage., 60, 119-134, 10.1016/S0378-3774(02)00162-2, 2003.
Garcia, M., Raes, D., Jacobsen, S. E., and Michel, T.: Agroclimatic constraints for rainfed agriculture in the Bolivian Altiplano, J Arid Environ., 71, 109-121, 10.1016/j.jaridenv.2007.02.005, 2007.
Garcia, M., Condori, B., and Del Castillo, C.: Agroecological and Agronomic Cultural Practices of Quinoa in South America, in: Quinoa: Improvement and Sustainable Production, edited by: Murphy, K., and Matanguihan, J., 25-46, 2015.
Garcia, M., and Alavi, G.: Bolivia, in: Atlas de Sequía de América Latina y el Caribe, edited by: Núñez Cobo, J., and Verbist, K., UNESCO y CAZALAC, La Serena, Chile, 29-42, 2018.
Garreaud, R., Vuille, M., and Clement, A. C.: The climate of the Altiplano: observed current conditions and mechanisms of past changes, Palaeogeogr. Palaeoclimatol. Palaeoecol., 194, 5-22, 10.1016/S0031-0182(03)00269-4, 2003.
Garreaud, R. D., and Aceituno, P.: Interannual rainfall variability over the South American Altiplano, J. Clim., 14, 2779-2789, 10.1175/1520-0442(2001)014<2779:Irvots>2.0.Co;2, 2001.
Geerts, S., Raes, D., Garcia, M., Mendoza, J., and Huanca, R.: Crop water use indicators to quantify the flexible phenology of quinoa (Chenopodium quinoa Willd.) in response to drought stress, Field Crops Res., 108, 150-156, 10.1016/j.fcr.2008.04.008, 2008.
Geerts, S., Raes, D., Garcia, M., Miranda, R., Cusicanqui, J. A., Taboada, C., Mendoza, J., Huanca, R., Mamani, A., Condori, O., Mamani, J., Morales, B., Osco, V., and Steduto, P.: Simulating Yield Response of Quinoa to Water Availability with AquaCrop, Agron. J., 101, 499-508, 10.2134/agronj2008.0137s, 2009.
Helman, D., Givati, A., and Lensky, I. M.: Annual evapotranspiration retrieved from satellite vegetation indices for the eastern Mediterranean at 250 m spatial resolution, Atmos. Chem. Phys., 15, 12567-12579, 10.5194/acp-15-12567-2015, 2015.
Holben, B. N.: Characteristics of maximum-value composite images from temporal AVHRR data, Int J Remote Sens, 7, 1417-1434, 10.1080/01431168608948945, 1986.
Huang, M., Piao, S., Ciais, P., Peñuelas, J., Wang, X., Keenan, T. F., Peng, S., Berry, J. A., Wang, K., Mao, J., Alkama, R., Cescatti, A., Cuntz, M., De Deurwaerder, H., Gao, M., He, Y., Liu, Y., Luo, Y., Myneni, R. B., Niu, S., Shi, X., Yuan, W., Verbeeck, H., Wang, T., Wu, J., and Janssens, I. A.: Air temperature optima of vegetation productivity across global biomes, Nature Ecology & Evolution, 3, 772-779, 10.1038/s41559-019-0838-x, 2019.
Iizumi, T., Luo, J.-J., Challinor, A. J., Sakurai, G., Yokozawa, M., Sakuma, H., Brown, M. E., and Yamagata, T.: Impacts of El Niño Southern Oscillation on the global yields of major crops, Nature Communications, 5, 3712, 10.1038/ncomms4712, 2014.

INE: Censo Agropecuario de Bolivia 2013, first ed., The National Institute of Statistics (INE) of Bolivia, La Paz, 143 pp., 2015.
IPCC: Climate Change 2013: The Physical Science Basis. Contribution of Working Group I to the Fifth Assessment Report of the Intergovernmental Panel on Climate Change, edited by: Stocker, T. F., Qin, D., Plattner, G.-K., Tignor, M., Allen, S. K., Boschung, J., Nauels, A., Xia, Y., Bex, V., and Midgley, G. F., Cambridge University Press, Cambridge, United Kingdom and New York, NY, USA, 1535 pp., 2013.
Ji, L., and Peters, A. J.: Assessing vegetation response to drought in the northern Great Plains using vegetation and drought indices, Remote Sens. Environ., 87, 85-98, 10.1016/S0034-4257(03)00174-3, 2003.
Karnieli, A., Agam, N., Pinker, R. T., Anderson, M., Imhoff, M. L., Gutman, G. G., Panov, N., and Goldberg, A.: Use of NDVI and Land Surface Temperature for Drought Assessment: Merits and Limitations, J. Clim., 23, 618-633, 10.1175/2009jcli2900.1, 2010.
Kogan, F., and Guo, W.: Strong 2015–2016 El Niño and implication to global ecosystems from space data, Int J Remote Sens, 38, 161-178, 10.1080/01431161.2016.1259679, 2017.
Kogan, F. N.: Application of vegetation index and brightness temperature for drought detection, Advances in Space Research, 15, 91-100, https://doi.org/10.1016/0273-1177(95)00079-T, 1995.
Kogan, F. N.: Satellite-Observed Sensitivity of World Land Ecosystems to El Niño/La Niña, Remote Sens. Environ., 74, 445-462, https://doi.org/10.1016/S0034-4257(00)00137-1, 2000.
Kutner, M. H., Nachtsheim, C., and Neter, J.: Applied linear regression models, McGraw-Hill/Irwin, 2004.
Moran, M. S., Clarke, T. R., Inoue, Y., and Vidal, A.: Estimating crop water deficit using the relation between surface-air temperature and spectral vegetation index, Remote Sens. Environ., 49, 246-263, https://doi.org/10.1016/0034-4257(94)90020-5, 1994.
El Niño and La Niña Years and Intensities: https://ggweather.com/enso/oni.htm, 2018.
Ochoa, A., Pineda, L., Crespo, P., and Willems, P.: Evaluation of TRMM 3B42 precipitation estimates and WRF retrospective precipitation simulation over the Pacific–Andean region of Ecuador and Peru, Hydrol. Earth Syst. Sci., 18, 3179-3193, 10.5194/hess-18-3179-2014, 2014.
Paredes-Trejo, F. J., Álvarez Barbosa, H., Peñaloza-Murillo, M. A., Moreno, M. A., and Farias, A.: Intercomparison of improved satellite rainfall estimation with CHIRPS gridded product and rain gauge data over Venezuela, 2016, 29, 20, 10.20937/atm.2016.29.04.04, 2016.
Paredes-Trejo, F. J., Barbosa, H. A., and Lakshmi Kumar, T. V.: Validating CHIRPS-based satellite precipitation estimates in Northeast Brazil, J Arid Environ., 139, 26-40, https://doi.org/10.1016/j.jaridenv.2016.12.009, 2017.
Ramirez-Rodrigues, M. A., Asseng, S., Fraisse, C., Stefanova, L., and Eisenkolbi, A.: Tailoring wheat management to ENSO phases for increased wheat production in Paraguay, Climate Risk Management, 3, 24-38, https://doi.org/10.1016/j.crm.2014.06.001, 2014.
Rencher, A. C.: Methods of Multivariate Analysis, John Wiley & Sons, New York, 1995.
Rivera, J. A., Marianetti, G., and Hinrichs, S.: Validation of CHIRPS precipitation dataset along the Central Andes of Argentina, Atmospheric Research, 213, 437-449, https://doi.org/10.1016/j.atmosres.2018.06.023, 2018.
Sánchez, N., Martínez-Fernández, J., González-Piqueras, J., González-Dugo, M. P., Baroncini-Turrichia, G., Torres, E., Calera, A., and Pérez-Gutiérrez, C.: Water balance at plot scale for soil moisture estimation using vegetation parameters, Agricultural and Forest Meteorology, 166-167, 1-9, https://doi.org/10.1016/j.agrformet.2012.07.005, 2012.
Santos, J. L.: The Impact of El Niño - Southern Oscillation Events on South America, Adv. Geosci., 6, 221-225, 10.5194/adgeo-6-221-2006, 2006.
Satgé, F., Bonnet, M.-P., Gosset, M., Molina, J., Hernan Yuque Lima, W., Pillco Zolá, R., Timouk, F., and Garnier, J.: Assessment of satellite rainfall products over the Andean plateau, Atmospheric Research, 167, 1-14, 10.1016/j.atmosres.2015.07.012, 2016.
Shinoda, M.: Seasonal phase lag between rainfall and vegetation activity in tropical Africa as revealed by NOAA

satellite data, Int. J. Climatol., 15, 639-656, 10.1002/joc.3370150605, 1995.
Thompson, L. G., Mosley-Thompson, E., and Arnao, B. M.: El Niño-Southern Oscillation events recorded in the stratigraphy of the tropical Quelccaya ice cap, Peru, Science, 226, 50-53, 10.1126/science.226.4670.50, 1984.
Tippett, M. K., Barnston, A. G., and Li, S.: Performance of Recent Multimodel ENSO Forecasts, J. Appl. Meteorol. Clim., 51, 637-654, 10.1175/jamc-d-11-093.1, 2012.
UNDP: Tras las huellas del cambio climático en Bolivia. Estado del arte del conocimiento sobre adaptación al cambio climático: agua y seguridad alimentaria, UNDP-Bolivia, La Paz, Bolivia, 144 pp., 2011.
UNISDR: Drought Risk Reduction Framework and Practices: Contributing to the Implementation of the Hyogo Framework for Action, United Nations secretariat of the International Strategy for Disaster Reduction (UNISDR), Geneva, Switzerland, 2009.
UNISDR: Making Development Sustainable: The Future of Disaster Risk Management. Global Assessment Report on Disaster Risk Reduction, United Nations Office for Disaster Risk Reduction (UNISDR), Geneva, Switzerland, 266, 2015.
van Loon, C. D.: The effect of water stress on potato growth, development, and yield, American Potato Journal, 58, 51-69, 10.1007/BF02855380, 1981.
Verbist, K., Amani, A., Mishra, A., and Cisneros, B. J.: Strengthening drought risk management and policy: UNESCO International Hydrological Programme's case studies from Africa and Latin America and the Caribbean, Water Policy, 18, 245-261, 10.2166/wp.2016.223, 2016.
Vicente-Serrano, S. M., Chura, O., López-Moreno, J. I., Azorin-Molina, C., Sanchez-Lorenzo, A., Aguilar, E., Moran-Tejeda, E., Trujillo, F., Martínez, R., and Nieto, J. J.: Spatio-temporal variability of droughts in Bolivia: 1955–2012, Int. J. Climatol., 35, 3024-3040, 10.1002/joc.4190, 2015.
Wilks, D. S.: Statistical Methods in the Atmospheric Sciences, second ed., Academic Press, 2006.
Yarleque, C., Vuille, M., Hardy, D. R., Posadas, A., and Quiroz, R.: Multiscale assessment of spatial precipitation variability over complex mountain terrain using a high-resolution spatiotemporal wavelet reconstruction method, J. Geophys. Res. Atmos., 121, 12,198-112,216, 10.1002/2016jd025647, 2016.
Zhou, J., and Lau, K.-M.: Does a monsoon climate exist over South America?, J. Clim., 11, 1020-1040, 10.1175/1520-0442(1998)011<1020:damceo>2.0.co;2, 1998.

APPENDIX

Table A1. Spatial location of the studied weather stations where gauged precipitation data are available, the stations that also present temperature maximum and minimum data indicate T on the column of temperature.

No	Station name	Latitude	Longitude	Altitude	Temperature
[1]	Ayo Ayo	-17.1	-68.0	3888	
[2]	Calacoto	-17.3	-68.6	3830	T
[3]	Collana	-16.9	-68.3	3911	T
[4]	El Alto Aeropuerto	-16.5	-68.2	4034	T
[5]	El Belen	-16.0	-68.7	3833	T
[6]	Oruro Aeropuerto	-18.0	-67.1	3701	T
[7]	Patacamaya	-17.2	-67.9	3793	
[8]	Salla	-17.2	-67.6	3500	
[9]	San Juan Huancollo	-16.6	-68.9	3829	
[10]	Santiago de Huata	-16.1	-68.8	3845	T
[11]	Tiahuanacu	-16.6	-68.7	3863	T
[12]	Viacha	-16.7	-68.3	3850	T

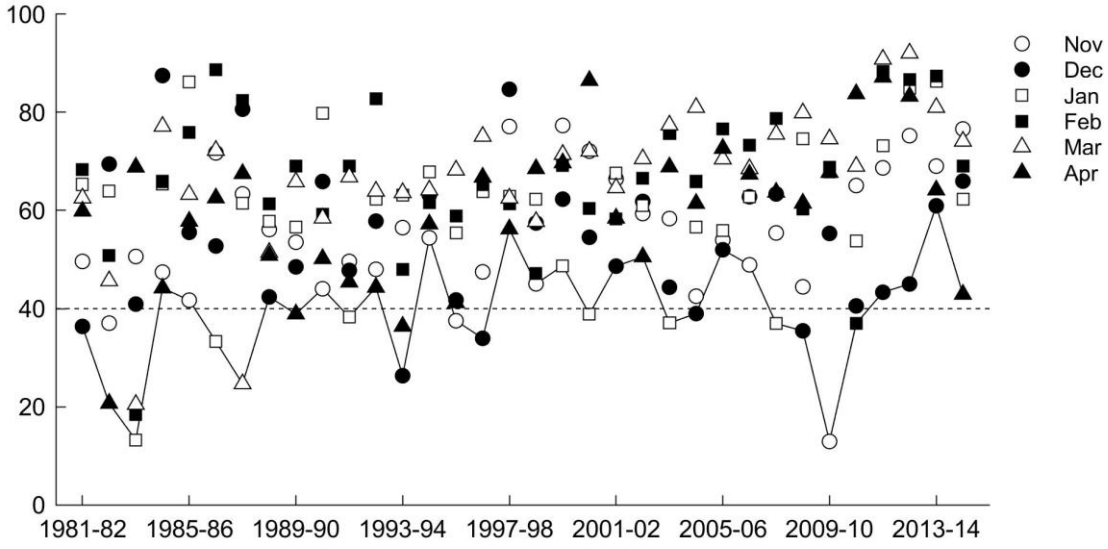

Fig. A1. Monthly mean of the VCI (%) from November 1981 to April 2015. Values below 40% (dashed line) represent a drought event.

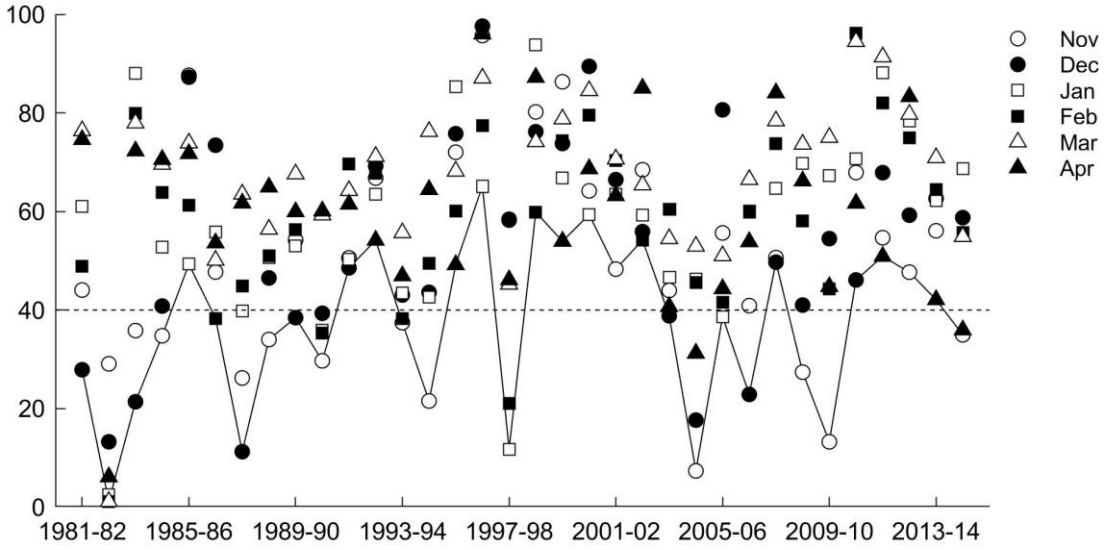

Fig. A2. Same as Fig. A1 but for the TCI.

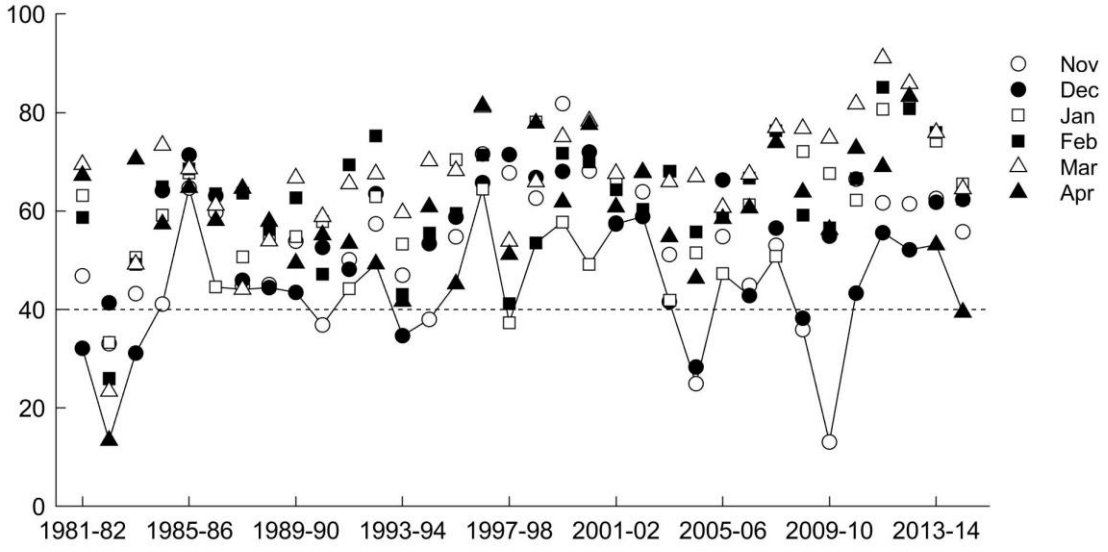

Fig. A3. Same as Fig. A1 but for the VHI.